Chemical Science

Accepted Manuscript

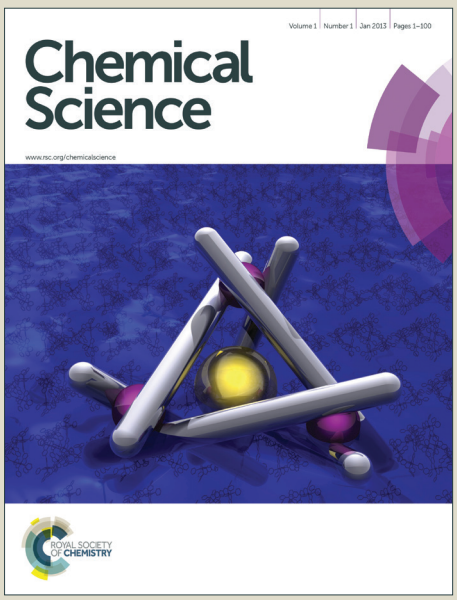

ROYAL SOCIETY OF CHEMISTRY

www.rsc.org/chemicalscience

Chemical Science

RSCPublishing

EDGE ARTICLE

The proton conduction mechanism in a material consisting of packed acids

Cite this: DOI: 10.1039/x0xx00000x

Takaya Ogawa,[a] Takashi Aonuma,[a] Takanori Tamaki,[a,b] Hidenori Ohashi,[a] Hiroshi Ushiyama,[c] Koichi Yamashita,[c] Takeo Yamaguchi[a,b,*]

Received 00th January 2012,
Accepted 00th January 2012

DOI: 10.1039/x0xx00000x

www.rsc.org/

Proton conduction due to acid–acid interactions is an important topic in a variety of fields, from materials science to biochemistry. We observed a distinctive proton conduction phenomenon for a material consisting of packed acids at the interface of zirconium sulphophenylphosphonate (ZrSPP) and sulphonated poly(arylene ether sulphone) (SPES). The proton in the composite was found active, while water, a general proton carrier, remained as immobile. Moreover, the conductivity of the composite material was higher than the sum of the individual conductivities of ZrSPP and SPES; particularly attributed to the packed acids present at the interface. We propose a "packed-acid mechanism" based on the results of *ab initio* calculations in order to explain such a significant and interesting behaviour of protons. During common proton conduction, pseudo-shuttling of a proton between a proton donor and acceptor is a general event that disrupts the reorientation phenomena; which is an important process associated with common proton conduction. Based on our results, it could be inferred that in packed acid materials, the acid–acid interaction eliminates the pseudo-shuttling (interception) and facilitates reorientation, resulting in successive proton conduction.

1. Introduction

The facilitation of proton conduction by acids is an important topic to both material science and biology[1-18]. For example, polymer electrolyte fuel cell (PEFC) and catalyst are significant applications highlighting the potential of proton transport in material sciences[1,2,12-18], while titratable amino acids drive many functions in biological systems, including the synthesis of adenosine triphosphate (ATP); which is triggered by proton movement through the proton channels[3-8]. Proton conduction supported by acids is recognized as an important area of materials science particularly because several proton conducting electrolytes are derived from various acids and are extremely useful in PEFCs[12-18]. In addition, proton diffusion via continuous Lewis acids on the surface of metal oxides has a number of applications, such as catalytic hydrogenation and photocatalytic dehydrogenation[1,2]. Despite its widespread use and importance, the fundamental mechanism associated with the effect of acids on proton conduction remains unknown[8,12-26]. In general, acids enhance proton conductivity by dissociating protons from them; by contrast, a negative charge on an acid in the absence of a proton attracts positively charged protons and disrupts proton conduction[14-18,21]. In addition to acids, water plays a key role in proton conduction as the proton carrier H_3O^+ because protons cannot exist alone in aqueous solution. Protons move in bulk water according to the Grotthuss mechanism, which involves necessary co-ordination constructed by the following two procedures: "hopping", in which a proton hops from a proton donor to an acceptor along a hydrogen bond (H-bond), and "reorientation", in which a H-bond is cleaved and the proton reorients to another proton acceptor[6,7,14,16-18,20,22-27]. The Grotthuss mechanism is typically regarded as the same as the well-known "structural diffusion" proton conduction mechanism, which presumably pertains not only to bulk water but also to various materials containing water and acids[4,18,20]. The diffusion occurs through co-ordination originating from reorientation in the second hydration shell followed by successive hopping events, involving the movement of $H_5O_2^+$ (the Zundel cation) and $H_9O_4^+$ (the Eigen cation) with several water molecules per proton[6,7,14,20,22-24,26,27]. Reorientation is generally the rate-determining step in proton conduction because of the overly strong H-bond formed around H^+. In structural diffusion, the reorientation is overcome by water reorientation in the second hydration shell through the fluctuation of the H-bond network formed between several water molecules. Since water is indispensable for structural diffusion, it fundamentally explains the decrease in the proton conductivity at a lower relative humidity (RH)[15-18]. Structural diffusion is a general proton-conduction mechanism associated with relatively small number of acid groups in the presence of sufficient water molecules. In contrast, an alternative proton conduction mechanism likely occurs for several acids in the solid state, such as proton conduction on a metal surface or in a proton channel, as discussed above[1-11]. In addition, there are several intriguing questions to be unravelled regarding the proton transport mechanism associated with biological cell membrane[8]. The fluctuations in the H-bond network result in a transient collective co-ordination of the water and acid molecules involved in proton conduction, which complicates the determination of mobility mechanisms at the molecular-level. Hence it could be envisaged that proton-conduction mechanisms involving acids are not fully understood[6-8,14,16-18,20,22-29].

In this study, a distinctive proton conduction phenomenon was observed at the nanoscale interface between synthesized as a

solid state material consisting of packed sulphonic acids. It could be seen that composites of various inorganic particles and polyelectrolytes have been fabricated in order to improve the performance of the polyelectrolyte[30-37]. In these studies, the distribution of inorganic particles in the polyelectrolyte was controlled to enhance the potential of the composite[31,32], however, the proton-conduction mechanism is either unknown or has not been discussed extensively. We have succeeded in finely dispersing zirconium sulphophenylphosphonate (ZrSPP) in sulphonated poly(arylene ether sulphone) (SPES) and in the resulting composite material, only proton movement was observed, while water, a general proton carrier, did not move. The behaviour of the protons and water molecules in the composite was evaluated separately via ^{2}H and ^{17}O magic-angle spinning solid-state nuclear magnetic resonance (MAS NMR) spectroscopy. Furthermore, the proton conductivity of the composite obtained was found higher than the sum of the individual conductivities of ZrSPP and SPES, indicating the presence of an intriguing proton-conduction mechanism at the ZrSPP–SPES interface. In order to investigate the proton conduction at the interface, we have performed the '*ab initio* molecular dynamics' (AIMD) calculations using models and we have found that the results obtained were consistent with the results of Fourier transform infrared (FT-IR) spectroscopy using attenuated total reflectance. We have identified the existence of another proton-conduction mechanism induced by acid–acid interactions that can well-explain the abnormal proton movements that occurs without the aid of water reorientation, enabling faster proton conduction at the interface of packed sulphonic acids.

2. Experimental and theoretical methods

2.1 Synthesis procedure

The interfaces were formed through the multipoint adsorption of the polymer electrolyte onto nanosized inorganic particles, as schematically illustrated in Fig. 1. The Stokes diameter of the mixed solution of SPES and (3-aminopropyl)-triethoxysilane zirconium

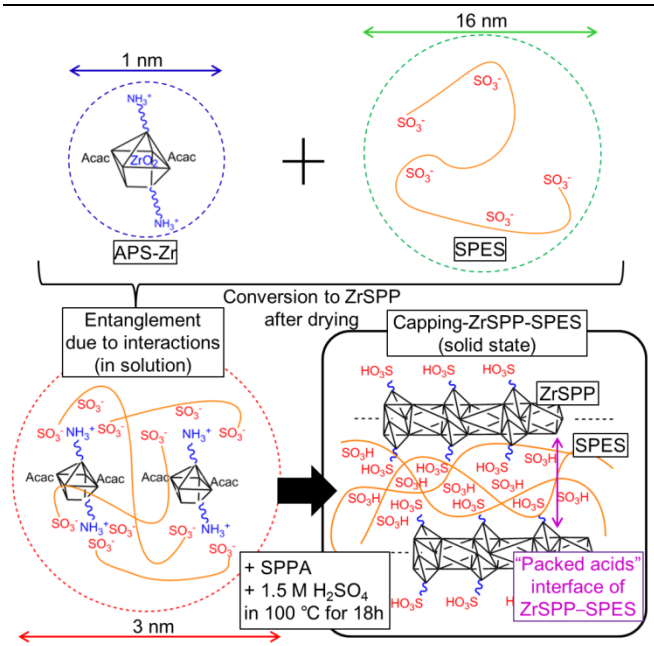

Figure 1. Conceptual procedure adopted for capping of ZrSPP–SPES.

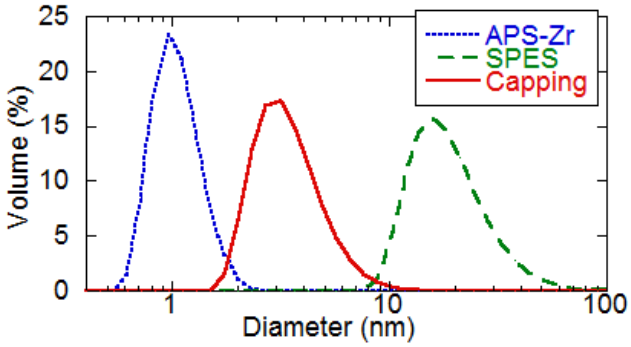

Figure 2. DLS results for APS–Zr, SPES, and the mix-solution of APS-Zr and SPES (after capping).

(IV) oxide (APS–Zr) precursor was smaller than that of SPES alone, as indicated by the dynamic light scattering (DLS) results (Fig. 2). The Stokes diameter of SPES decreased from approximately 16 nm to approximately 3 nm, suggesting that SPES was entangled with APS–Zr; hereafter, we refer to this multipoint adsorption as "capping". This solution was cast onto a glass plate and dried to form a solid electrolyte. In situ conversion of APS–Zr to ZrSPP through a mild route resulted in an electrolyte that possessed nanointerfaces (capping-ZrSPP–SPES)[38]. The *in situ* conversion of APS–Zr to ZrSPP was confirmed by FT-IR and inductively coupled plasma atomic emission spectrometry (ICP–AES) (see section I-III in the Electronic Supporting Information (ESI) for more details).

We synthesized another electrolyte for comparison by mixing SPES and the previously synthesized ZrSPP (simple-mixing-ZrSPP–SPES) as described previously[30,33].

2.2. Calculation methods and models

We performed *ab initio* calculations to investigate the proton-conduction mechanism of packed acids at the ZrSPP–SPES interface using the SIESTA (Spanish Initiative for Electronic Simulations with Thousands of Atoms) 2.0.1 software package[39]. The electronic structure is represented within the generalized gradient approximation of density functional theory using the RPBE (Revised Perdew–Burke–Ernzerhof) functional[40]. A double-zeta split-valence basis set with polarization orbitals was used[41]. We applied the nudged elastic band method to find the activation energies (E_a)[42-44] of hopping and reorientation.

We have modelled the interface with one layer of ZrSPP, which is an inorganic layered crystal and benzenesulphonic acid (BS) as SPES. Several water molecules were allocated to the interface, and 42 patterns of the interface structure were optimized to construct the H-bond network (Fig. 3). The number of water molecules per SO_3H, λ, is 0–9. A low λ value leads to a short distance between the ZrSPP and the BS, and a high density of sulphonic acid, which simulates the packed-acid structure presented in the study. The models were calculated with the value of the net charge set to 0. More details, including the method for constructing the models and determining E_a, are shown in Section IV in the ESI.

3. Experimental results and discussions

3.1. The large surface area of the ZrSPP–SPES interface in the capping-ZrSPP–SPES sample

Transmission electron microscopy (TEM) images revealed that ZrSPP was homogeneously dispersed in the capping-ZrSPP–SPES sample. The dark regions of these images correspond to ZrSPP, whereas the grey regions correspond to SPES (Fig. 4, other images

are in Section II in ESI). However, the simple-mixing-ZrSPP–SPES interface contained large ZrSPP particles of approximately 1–3 μm in size (see Fig. S1).

Thus, the capping-ZrSPP–SPES offer significantly larger surface area at the ZrSPP–SPES interface, compared to the interface formed by simple-mixing of ZrSPP–SPES. Hence, it is apparent from the TEM images that the capping method is more efficient and could generate a better ZrSPP–SPES composite compared to simple mixing method.

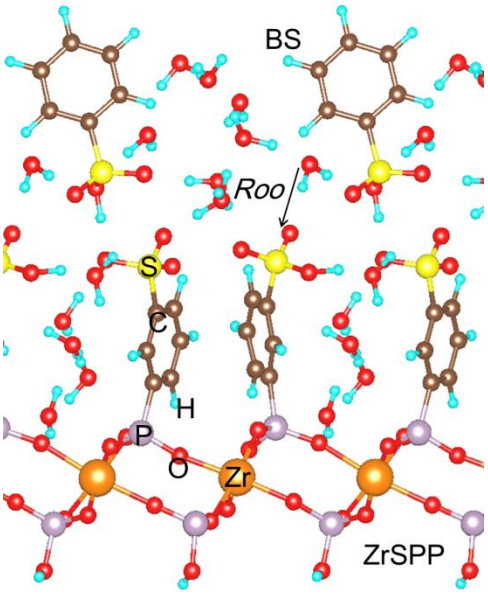

Figure 3. The ZrSPP–SPES model is shown (λ = 4.33). The ZrSPP layer is underneath, and SPES is modeled as BS and placed above the ZrSPP with the water molecules. The colour scheme in the figures is the same throughout this paper. In addition, *Roo* (black arrow) is shown.

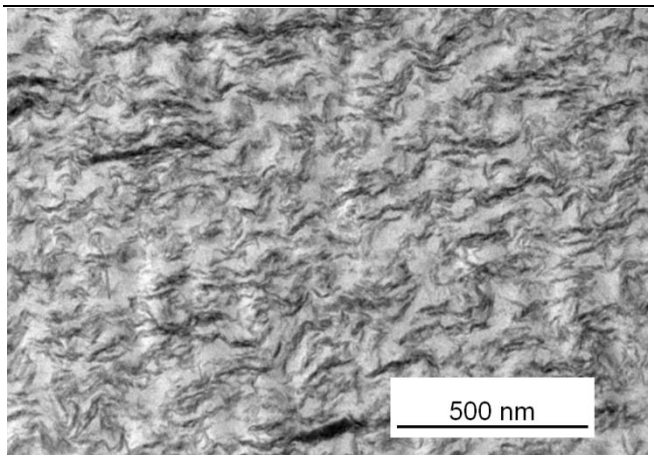

Figure 4. TEM image showing that the capping-ZrSPP–SPES sample has a large surface area.

3.2. Characterization of the structure of capping-ZrSPP–SPES by FT-IR

The characteristic properties of the ZrSPP–SPES interface were investigated by FT-IR spectroscopy (full FT-IR spectra are shown in Fig. S2). In the FT-IR spectra of the capping-ZrSPP–SPES samples, the O–S–O asymmetric stretching vibration[45] shifted to a higher wavenumber—ZrSPP: 1233 cm^{-1}; SPES: 1233 cm^{-1}; compared to simple-mixing-ZrSPP–SPES: 1234 cm^{-1}; and capping-ZrSPP–SPES: 1240 cm^{-1} (Fig. 5). Based on the TEM results, the high wavenumber for O–S–O in capping-ZrSPP–SPES is likely due to the increased ZrSPP–SPES interface. In general, sulphonic acid groups generate a strong H-bond, which leads to a stable energy level and a low O–S–O wavenumber; thus, a high wavenumber implies a high energy level of the sulphonic acid group due to weak H-bond. The acid–acid interaction occurs when sulphonic acid groups are locally concentrated and interact with each other (see Sections V–VII in the ESI). The O–S–O wavenumber shifts to a higher value in the case that sulphonic acids confront each other, which generates a weak H-bond because of the low proton affinity of sulphonic acid (see Section V–VII in the ESI). NMR measurements in Section 3.4 also indicate the high concentration of sulphonic acids in capping-ZrSPP–SPES (see Section 3.4 below). The capping method adopted in this study has resulted in a structure with highly interacting sulphonic acid groups, which created weaker H-bond. Hence, it could be envisaged that the sulphonic acid groups at the ZrSPP–SPES interface are primarily concentrated locally and generate weaker H-bond.

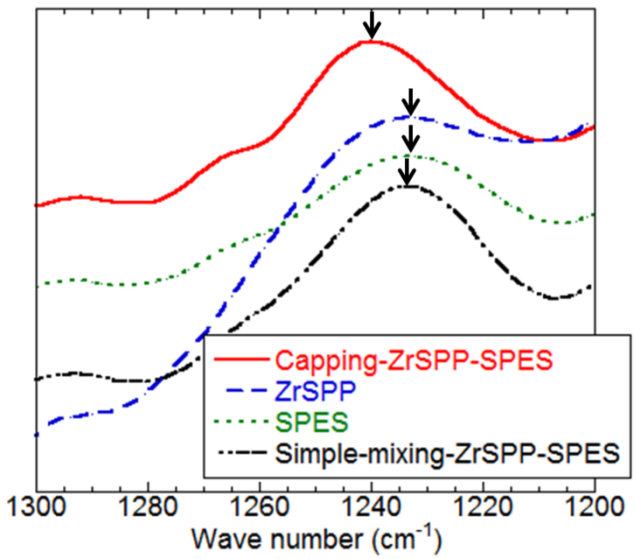

Figure 5. FT-IR spectra of SPES, ZrSPP, capping-ZrSPP–SPES, and simple-mixing-ZrSPP–SPES samples.

3.3. High proton conductivity of the capping-ZrSPP–SPES interface

The proton conductivities of each material was measured by AC impedance spectroscopy at 90 °C and various relative humidity conditions (Fig. 6). Notably, the conductivity of capping-ZrSPP–SPES was higher at various values of RH than the sum of the conductivities of each single material or the conductivity of the simple-mixing-ZrSPP–SPES sample. E_a of proton conductivity of capping-ZrSPP–SPES at 80, 60, and 40% RH (60–90 °C) were 13, 16, and 23 kJ/mol, while these of SPES were 17, 19, and 28 kJ/mol, respectively (These values were calculated using the Nernst–Einstein equation[46]. See Section III in ESI). Detailed discussion of these values is given in Section 4.5.2. In particular, the values of ZrSPP-SPES were

lower than those of SPES. The capping-ZrSPP–SPES and the others differ in the area of the ZrSPP–SPES interface with packed acids, as determined by TEM and FT-IR. Therefore, this high proton conductivity and low E_a is attributed to packed acids present at the ZrSPP–SPES interface. The proton behaviour at the ZrSPP–SPES interface is examined in the following sections.

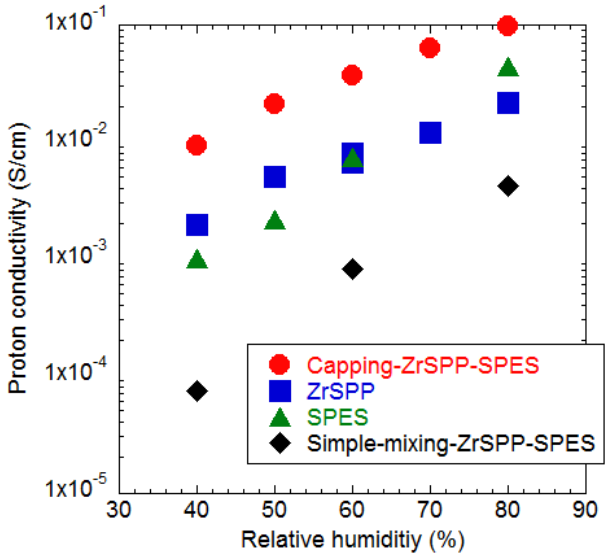

Figure 6. Proton conductivity of each material at 90 °C and various values of RH.

3.4. Proton behaviour in capping-ZrSPP–SPES

To investigate the proton and water behaviours in the composites, ^{2}H- and ^{17}O-MAS NMR were used. The composites were incubated in D_2O at 100% RH for three days that will result in the exchange of the protons belong to sulphonic acid and adsorbed water, and thus the ^{2}H-MAS NMR spectrum includes only the signal of the mobile proton. Similarly, for ^{17}O-MAS NMR analysis, the composite was incubated in $H_2{}^{17}O$ at 100% RH for three days.

The ^{2}H-MAS NMR spectra of the capping-ZrSPP–SPES and the simple-mixing-ZrSPP–SPES samples measured at 47.3, –15.3, and –38.8 °C demonstrated that the peak observed in the capping-ZrSPP–SPES sample maintained its shape at low temperature (Fig. 7a), whereas the peak observed in the simple-mixing-ZrSPP–SPES sample broadened and decreased (Fig. 7b). The peak shape in the capping-ZrSPP–SPES sample at –38.8 °C indicates that the proton remained as active as at 47.3 °C, while the small and broad peak in the simple-mixing-ZrSPP–SPES sample at –38.8 °C suggests that proton mobility decreased due to freezing of water at this low temperature. In addition, the behaviour of the water in the capping-ZrSPP–SPES sample was analysed by ^{17}O-MAS NMR. The ^{17}O-MAS NMR spectrum revealed that the peak diminished at –38.8 °C, suggesting that the water at the interface became frozen (Fig. 7c). Therefore, the protons in the capping-ZrSPP–SPES samples retained their mobility at –38.8 °C, even though water molecule, a general carrier of protons, did not move. This proton behaviour cannot be explained by the common proton-conduction mechanism and suggests that another proton-conduction mechanism occurs in the capping-ZrSPP–SPES sample. This unusual proton behaviour is explained by the proton conduction mechanism proposed based on the theoretical results.

In addition, the ^{2}H peak in capping-ZrSPP–SPES was at a lower magnetic field than the ^{2}H peak in simple-mixing-ZrSPP–SPES, originating from the lower field of sulphonic acids compared with water. In other words, ^{2}H in capping-ZrSPP–SPES interacted with sulphonic acids more strongly than in simple-mixing-ZrSPP–SPES. These results support the existence of highly concentrated sulphonic acids in capping-ZrSPP–SPES, which confirms the FT-IR results in Section 3.2.

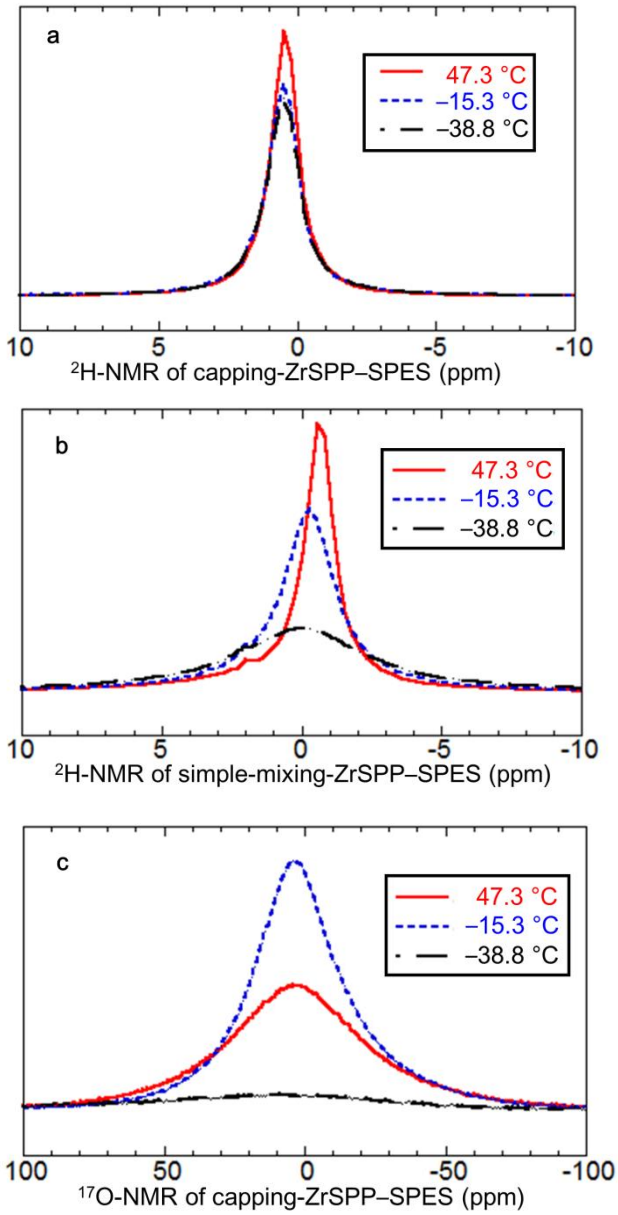

Figure 7. ^{2}H-NMR analysis of (**a**) capping-ZrSPP–SPES and (**b**) simple-mixing-ZrSPP–SPES and (**c**) ^{17}O-NMR analysis of capping-ZrSPP–SPES at 47.3, –15.3, and –38.8 °C. The larger and sharper peak of ^{17}O at –15.3 °C than that at 47.3 °C is due to a characteristic of the instrument in which the intensity increases at lower temperature with the ^{17}O quadrupole[47].

4. Theoretical results and discussions

4.1. The consistency of the calculation model

The consistency of the model for capping-ZrSPP–SPES is experimentally supported by FT-IR. The average wavenumber calculated for O–S–O in the models with λ values of 9, 1-5, and 0 was 1117, 1157, and 1242 cm^{-1}, respectively. Thus, the model with few water molecules, *i.e.*, with packed acids, is more similar to capping-ZrSPP–SPES than the other models with many water molecules, *i.e.*, with loosely associated acids. The O–S–O wavenumber shifts to a higher value in the case that sulphonic acids confront each other, and interact to generate a weak H-bond, as proposed theoretically (see Sections V–VII in the ESI). Comparison of the packed and loosely associated acid structures revealed the existence and effect of the acid–acid interactions in proton conduction associated with the material consisting of packed acids.

4.2. Important factor for determining the proton conductivity

The Nernst–Einstein equation clearly demonstrates that proton conductivity depends on E_a[46]. We sought to determine the nature of the proton conduction by investigating important factors related to E_a using optimized structures. The E_a values for the hopping and reorientation steps were calculated for more than 100 patterns. The results demonstrated that E_a depends on the distance between the two oxygen atoms of the proton donor and acceptor along an H-bond (*Roo*, Fig. 3). In Fig. 8, hopping is likely to occur if *Roo* is < 2.6 Å (Fig. 8a), whereas reorientation occurs preferentially if *Roo* is > 2.6 Å (Fig. 8b). Hence, hopping and reorientation are a trade-off in terms of *Roo*; both short and long *Roo* distances are necessary for proton conduction.

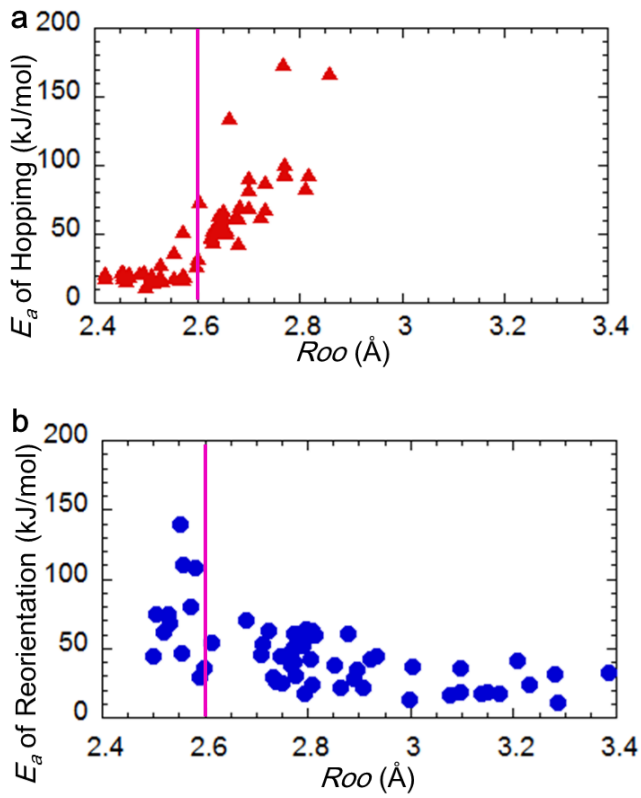

Figure 8. E_a values for (**a**) hopping and (**b**) reorientation are plotted against *Roo*, revealing a clear dependence.

4.3 *Roo* of classified groups in the ZrSPP–BS model

The *Roo* distances in the optimized structure are classified into several groups (Fig. 9) based on the oxygen atom of the H-bond donor and acceptor, in which X→Y represents the H-bond formed from X to Y. As an attempt to further understand the relationship between the acid–acid interaction and *Roo*, the probability that *Roo* is shorter than 2.6 Å in each classified group ($P_{<2.6}$) was calculated using the following equation:

$$P_{<2.6} = \frac{(<2.6)}{(\text{Total})}$$

in which "< 2.6" and "Total" represent the number of H-bonds whose *Roo* values are < 2.6 Å in each classified group (Fig. 9a, b) and the total number of H-bonds in each group, respectively. As shown in Fig. 8, a high $P_{<2.6}$ indicates that hopping occurs easily but reorientation is difficult, while a low $P_{<2.6}$ suggests the opposite. The $P_{<2.6}$ in the optimized structures for each group is shown in Table 1. It could be understood from Table 1 that H-bond formed from proton donor, SO_3H and H_3O^+, to proton acceptor, SO_3^- and H_2O, has a higher $P_{<2.6}$ value > 60%, suggesting that S1, S2, H1, and H2 groups cause hopping. In contrast, H-bond formed from proton donor to proton donor has a quite low value of $P_{<2.6}$, 0%, indicating that S3 and H3 groups facilitates reorientation. These data explain the proton behaviours determined in the AIMD calculations that are described in the next section.

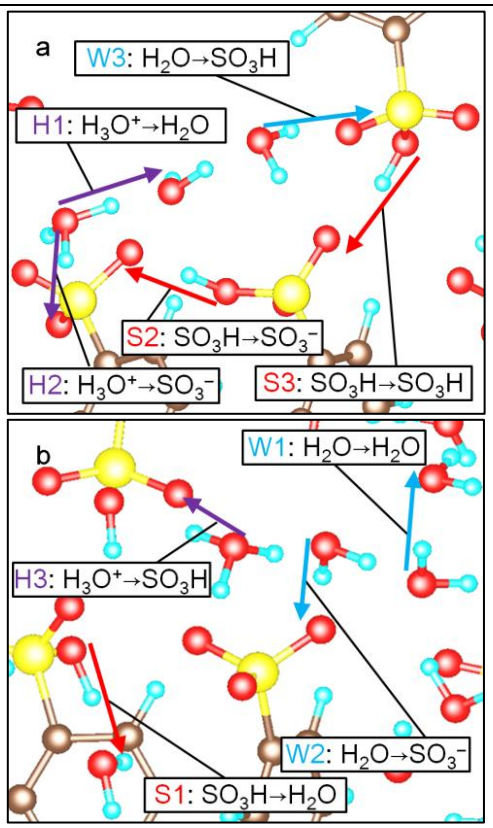

Figure 9. (**a**)The group sets W3, H1, H2, S2, and S3. (**b**) The group sets W1, W2, H3, and S1.

Table 1. The $P_{<2.6}$ values for each classified group in Fig. 9a and 9b.

Group	Subgroup	Component	$P_{<2.6}$(%)
From donor to acceptor	S1	$SO_3H \rightarrow H_2O$	74.1
	S2	$SO_3H \rightarrow SO_3^-$	66.7
	H1	$H_3O^+ \rightarrow H_2O$	86.8
	H2	$H_3O^+ \rightarrow SO_3^-$	61.8
From donor to donor	S3	$SO_3H \rightarrow SO_3H$	0
	H3	$H_3O^+ \rightarrow SO_3H$	0
From proton acceptor	W1	$H_2O \rightarrow H_2O$	17
	W2	$H_2O \rightarrow SO_3^-$	5.9
	W3	$H_2O \rightarrow SO_3H$	1.8

4.4 The proton conduction mechanism

We performed an AIMD calculation at 363 K (90 °C), the same temperature used for the measurement of proton conductivity in experimental section to demonstrate proton conduction at the interface using a Nosé thermostat[48]. Snapshots of the AIMD are shown in Fig. 10 and Fig. 11. We have rationalized the behaviour of the protons in the AIMD based on the above discussion of the classified groups and $P_{<2.6}$ values in the optimized structures in Table 1.

4.4.1 In the structure with loosely associated acids. First, we investigated the proton behaviour in the region composed of individual acid groups surrounded by water, *i.e.*, the structure with loosely associated acids, which occurs without acid–acid interactions. This region often appears in the model with many water molecules, which contains many proton acceptors and few proton donors. During the AIMD, we observed many resonances of $SO_3H \rightarrow H_2O$ (S1)/$H_3O^+ \rightarrow SO_3^-$ (H2) and $H_3O^+ \rightleftarrows H_2O$ (H1), *i.e.*, groups of H-bond formed from proton donor to proton acceptor (snapshots are shown in Fig. 10). Proton donor, SO_3H and H_3O^+, becomes proton acceptor, SO_3^- and H_2O, after proton hopping occurs to acceptor (proton dissociation), while proton acceptor becomes proton donor after proton hopping occurs from donor (proton acceptation). Therefore,

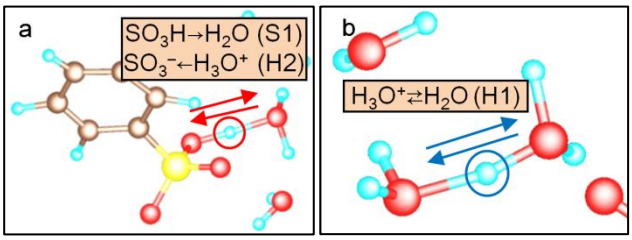

Figure 10. The snapshots during AIMD within the structure with loosely associated acids. (**a**) The group $SO_3H \rightarrow H_2O/H_3O^+ \rightarrow SO_3^-$ are resonance structures. The red-circled proton is trapped within the water and sulphonic acid because of the high $P_{<2.6}$ values of S1 and H2. (**b**) $H_3O^+ \rightleftarrows H_2O$ are resonance structures. The blue-circled proton shuttles between the water molecules.

the group of H-bond formed from proton donor to acceptor remains as the same even after hopping, and continues to induce hopping and disrupt reorientation, resulting in incompletion and interruption of proton conduction. In Fig. 10a, the red-circled proton shuttles and is trapped within sulphonic acid and water because of the high $P_{<2.6}$ values of S1 and H2. Hereafter, we denote this back-and-forth hopping, in which a proton shuttles and is trapped between the proton donor and acceptor, as "pseudo-shuttling". In Fig. 10b, the proton is also involved in pseudo-shuttling between the water molecules and the formed $H_5O_2^+$ because of the high $P_{<2.6}$ value of H1. The high $P_{<2.6}$ values result in excessively strong H-bonding and disturbed reorientation; the proton donors, H_3O^+ and SO_3H, strongly bind to the proton acceptors, H_2O and SO_3^-. Thus, the pseudo-shuttling results in the region composed of individual acids supports the earlier notion that Coulombic attraction between a proton and an acid in the absence of other protons restricts proton migration as indicated Fig. 10a. The water molecules must provide a gap between the proton and acid for the proton to escape the Coulombic attraction that arises from the acid's lack of a proton. In addition, the pseudo-shuttling illustrated in Fig. 10b; which supports the concept that the necessary reorientation procedure does not occur at the first hydration shell. In order to facilitate reorientation, the strength of the H-bond in $H_5O_2^+$ should be "diluted" by multiple water molecules, allowing reorientation happening in the second hydration shell.

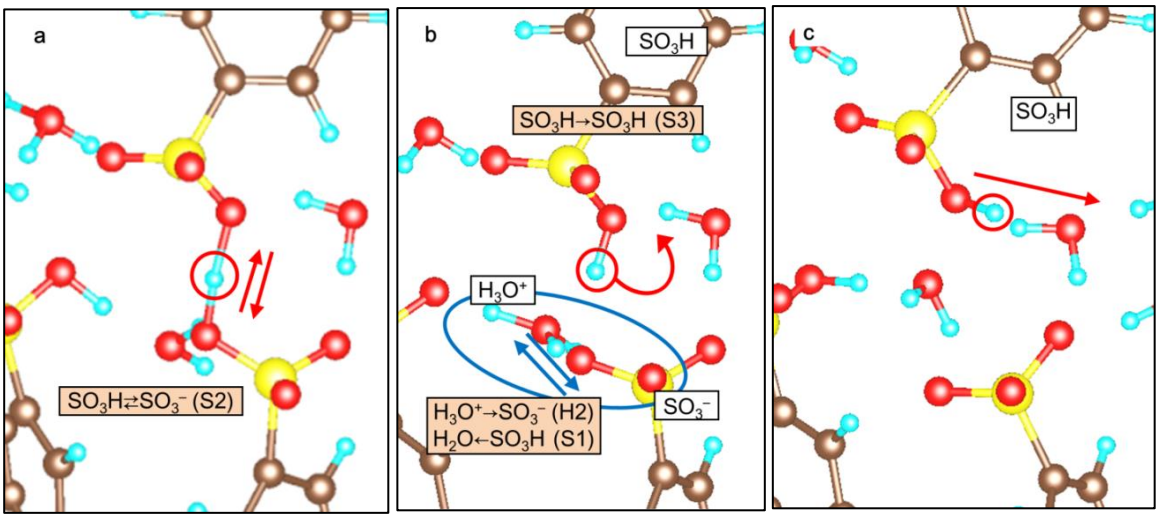

Figure 11. Snapshots during AIMD of the structure with packed acids. The proton behaviours in the packed-acid mechanism are shown. (**a**) The red-circled proton in SO_3H hops to the next SO_3^- in the pseudo-shuttling of the strong H-bond in $SO_3H \rightarrow SO_3^-$ (S2). (**b**) H_3O^+ and SO_3^-in the blue circle create the resonance structure $H_3O^+ \rightarrow SO_3^-/SO_3H \rightarrow H_2O$. The H-bond of the red-circled proton is intermittently weakened because the strongly H-bonded $SO_3H \rightarrow SO_3^-$ converts to $SO_3H \rightarrow SO_3H$ with a $P_{<2.6}$ value equal to 0%. (**c**) Thus, the red-circled proton reorients to another water molecule.

Therefore, the proton conduction mechanism in this region is basically structural diffusion. The gap and dilution requirement account for the experimental data demonstrating the significant decrease in the proton conductivity of an electrolyte at low RH[16-18]. Furthermore, compared with the $P_{<2.6}$ value of $H_2O \rightarrow H_2O$ (W1), sulphonic acid is more inclined than water (W2, W3) to repel protons. This repulsion implies that sulphonic acid has a low proton affinity and rarely participates in the proton pathway. In $H_3O^+ \rightarrow SO_3^-$ (H2), a proton hops to a sulphonic acid molecule and initiates pseudo-shuttling. Therefore, in the region composed of individual acids, the acids do not contribute to proton conduction after proton dissociation; but their role is only to increase the concentration of protons. Proton conduction requires several water molecules to construct a proton path.

4.4.2 In the structure with packed acids. In contrast to individual-acid regions, a distinctive proton-conduction mechanism can be identified in regions containing packed-acids with acid–acid interactions, which appears in the model with low λ (snapshots are shown in Fig. 11). In such regions, pseudo-shuttling can also be detected between the proton donor and acceptor; the red-circled proton hops back-and-forth from SO_3H to SO_3^- (Fig. 11a). However, this pseudo-shuttling is eliminated by the H-bonds formed from other proton donors; H_3O^+ and SO_3^- (within the blue circle) take the resonance forms $H_3O^+ \rightarrow SO_3^-$ (H2)/$H_2O \rightarrow SO_3H$ (S1) (Fig. 11b). Thus, an initially strong H-bond, $SO_3H \rightarrow SO_3^-$ (S2), is intermittently changed to a weak H-bond, $SO_3H \rightarrow SO_3H$ (S3), with a $P_{<2.6}$ value of 0%, which enables reorientation (Fig. 11c, red-circled proton). In other words, group of H-bond formed from proton donor to acceptor is converted to group of H-bond formed from proton donor to donor intermittently, eliminating pseudo-shuttling. We refer to the elimination of pseudo-shuttling by acid–acid interactions as an "interception". The weak H-bond of $SO_3H \rightarrow SO_3H$ (S3) arises from the low proton affinity of each SO_3H. Hence, the SO_3H reorients freely, couples with another proton acceptor during pseudo-shuttling to cause another interception, and successively facilitates the next reorientation. Thus, the role of acid–acid interactions is to generate a weak H-bond by interception. In the above scenario, SO_3H and SO_3^- can be replaced with H_3O^+ and H_2O, respectively, because they have nearly equal $P_{<2.6}$ values. A schematic representation of the proton conduction mechanism in a region with packed acids is shown in Fig. 12. First, pseudo-shuttling† is eliminated by the interception from a proton donor* (Fig. 12a). The released proton donor** reorients to another proton acceptor and causes the next interception to eliminate further pseudo-shuttling†† (Fig. 12b). Sequential proton conduction occurs through these steps (Fig. 12c). The event can be repeated without reaching a "dead end" in successive proton paths composed of proton donors/acceptors, which enables a proton to permeate a membrane in biological systems or an electrolyte for an application. Consequently, we propose this scheme as the "packed-acid mechanism". These steps are enabled by the large quantity of proton donors, H_3O^+ and SO_3H, in a packed-acid structure, in contrast to individual-acid regions, which contain only a few proton donors. The important criterion enabling the packed-acid mechanism is the packed-acid structure, which includes some water molecules. Therefore, the packed-acid mechanism is not a specific mechanism that occurs only at the ZrSPP–SPES interface but could occur in any structure with packed acids.

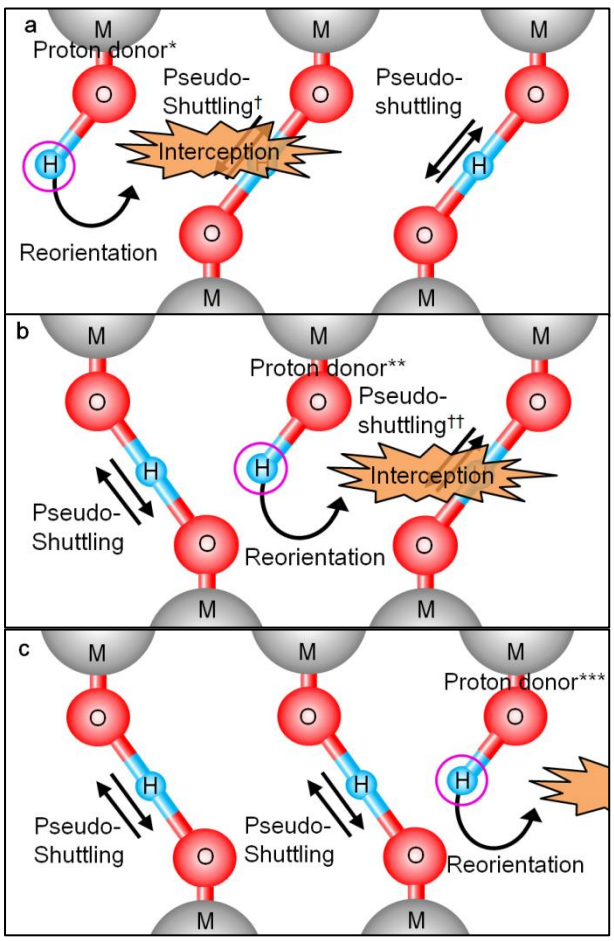

Figure 12. "M and O" stands for sulfonic acid group in the absence of proton or water. (**a**) Proton pseudo-shuttling (†) is eliminated by the proton donor (*). (**b**) The released proton donor (**) reorients and eliminates pseudo-shuttling (††). (**c**) The released proton donor (***) eliminates the next pseudo-shuttling.

SO_3^- accepts H^+ from SO_3H and H_3O^+ because of the high $P_{<2.6}$ values of S2 and H2 induced by its strong acidity, whereas SO_3^- does not couple with H_2O (W2). This phenomenon promotes pseudo-shuttling, which suggests that SO_3^- cannot participate in the proton path in general proton conduction. However, pseudo-shuttling in S2 and H2 can be eliminated in the packed-acid mechanism; the proton donors, H_3O^+ and SO_3H, "activate" the SO_3^- as a proton-conducting path. This role derives from the acid–acid interactions via interception.

Since hopping and reorientation are originated from the Grotthuss mechanism, it could be considered that the packed-acid mechanism is also derived from the Grotthuss mechanism. Therefore, although the Grotthuss mechanism is typically regarded as the same as structural diffusion[4,18,20], it might be divided into structural diffusion and the packed-acid mechanism. The major difference between structural diffusion and the packed-acid mechanism is the origin of reorientation. In structural diffusion, a fluctuation of the H-bond network among the water molecules causes a reorientation in the second hydration shell, not the first hydration shell. In this system based on the packed-acid mechanism, the acid–acid interaction causes a reorientation in first hydration shell as well. The sulphonic acid density (*i.e.*, λ) necessary to initiate the packed-acid mechanism is likely 0.3–3 (see Section IX in ESI). This value should be a basic index to characterize the packed-acid mechanism experimentally.

4.5 Comparison of experimental and theoretical results

We explain the experimental results, such as the unusual proton behaviour and high proton conductivity in capping-ZrSPP–SPES, in

the context of the theoretical results. First, a brief summary of the experimental results is shown, which is followed by a discussion.

4.5.1 A brief summary of the experimental results. The capping-ZrSPP–SPES sample had a large surface area at the ZrSPP–SPES interface, as determined by TEM. The FT-IR results demonstrated that the O–S–O wavenumber was highest for capping-ZrSPP–SPES, which indicated that the ZrSPP–SPES interface included a weak H-bond generated by packed acids. The NMR results show the ^{2}H peak at lower field, suggesting the existence of packed acids in capping-ZrSPP–SPES, in agreement with the FT-IR results. The capping-ZrSPP–SPES sample exhibited a higher proton conductivity at various values of RH than the sum of the conductivities of each single material or the conductivity of the simple-mixing-ZrSPP–SPES sample. In particular, the E_a of proton conductivity of ZrSPP–SPES at 90 °C and various values of RH were lower than those of SPES. The NMR results demonstrated that the proton mobility in the capping-ZrSPP–SPES sample remained high without water movement, which cannot be explained by the common conduction mechanism, suggesting that another proton-conduction mechanism occurs in capping-ZrSPP–SPES.

4.5.2 Explanation of the experimental results based on the theoretical results. In the packed-acid mechanism, the reorientation is facilitated by the acid–acid interaction without the aid of water movement. Thus, only the proton can move in the pool containing the water and sulphonic acid groups without the movement of the water molecules. Therefore, the packed-acid mechanism explains the NMR results for capping-ZrSPP–SPES, which revealed that only the proton moves, whereas water, the proton carrier, does not move. Our FT-IR and NMR results demonstrate that the structure of the capping-ZrSPP–SPES interface is similar to that of packed acids. The experimental FT-IR results suggest that the capping method generates a weak H-bond network for the proton donor interaction, *i.e.*, the interception at the ZrSPP–SPES interface (acid–acid interaction). A weak H-bond with interception, which eliminates pseudo-shuttling, is the most important factor in the packed-acid mechanism. The values of E_a for proton conductivity in capping-ZrSPP–SPES and SPES were 13–28 kJ/mol, attributed to the H-bond strength, *i.e.*, cleavage of the H-bond[23]. In particular, E_a of capping-ZrSPP–SPES was lower by 3–5 kJ/mol than E_a of SPES. Previous research proposed that high density of acid (acid–acid interaction) leads to a low E_a [49]. Therefore, the lower E_a can be considered to result from a weakened H-bond by acid–acid interaction. Hence, these results validate that the packed-acid mechanism occurs in the capping-ZrSPP–SPES sample and leads to distinctive proton conduction, as demonstrated by the NMR results. In the packed-acid mechanism, a weak H-bond facilitates the general rate-determining step: reorientation. In addition, hopping can occur in a concerted manner and can also be facilitated through this mechanism (see Section VI, VIII in ESI). Because the packed-acid mechanism facilitates both hopping and reorientation, we attribute the high proton conductivity and the low E_a of the capping-ZrSPP–SPES sample to a packed-acid mechanism.

As explained in Section 4.4.2, a method to generate a structure of packed acids and activate the packed-acid mechanism is not limited to the capping method and can be extended to any method that can concentrate acids sufficiently to construct a weak H-bond network among the proton donors. For example, self-assembled polymer electrolytes can construct such similar structure as that of packed acids.

The proton behaviour in the packed-acid mechanism exhibits similarities with selectivity of proton channels; in a proton channel comprising water molecules frozen in a narrow pore or several titratable amino acids, where only proton can move, while other ions cannot[3-7]. Thus, a packed-acid mechanism may be the origin of the proton selectivity in proton channels. Moreover, the high proton conductivity produced by the packed-acid mechanism is significantly attractive because low proton conductivity at low RH is a severe limitation in several applications, such as the use of electrolytes in clean-energy technologies[12-18].

5. Conclusions

Distinctive proton behaviour was detected at capping-ZrSPP–SPES interfaces with packed acids structure. The proton conductivity of the capping-ZrSPP–SPES exceeded the sum of the individual conductivities of ZrSPP and SPES as well as the conductivity of ZrSPP–SPES sample prepared by simple-mixing method. In particular, the E_a of proton conductivity of ZrSPP–SPES at 90 °C and various values of RH were lower than those of SPES. Moreover, in the capping-ZrSPP–SPES sample, the NMR results demonstrated that the mobility of proton remains same from –38.8 °C to 47.3 °C, whereas water, the general proton carrier, did not move. This distinctive proton behaviour is due to packed sulphonic acid, as indicated by *ab initio* calculations. The capping-ZrSPP–SPES interface was modelled by a structure with packed acids; and this model is supported by both experimental and theoretical FT-IR results. Based on the experimental results and theoretical calculations, we propose the existence of a 'packed-acid mechanism': originating from the acid–acid interactions in the material consisting of packed acids causing interceptions that eliminate pseudo-shuttling, followed by the generation of a weak H-bond network that facilitates proton conduction. The proton behaviour as per the packed-acid mechanism, such as the movement of proton alone, without the aid of water molecules, is in agreement with the experimental NMR results. Most significantly, the rate-determining step 'reorientation' is facilitated by the formation of a weak H-bond in the packed-acid mechanism, explaining such a high proton conductivity and a low E_a observed in capping-ZrSPP–SPES.

Acknowledgements

The authors acknowledge helpful assistance with solid-state NMR measurements from Dr. Kazuhiro Kamiguchi and Dr. Hideto Imai of Nissan Arc, Ltd. and with TEM analysis from the Centre for Advanced Materials Analysis at the Tokyo Institute of Technology.

Notes and references

[a] Chemical Resources Laboratory, Tokyo Institute of Technology, R1-17, 4259 Nagatsuta, Midori-ku, Yokohama 226-8503, Japan.

[b] Kanagawa Academy of Science and Technology, R1-17, 4259 Nagatsuta, Midori-ku, Yokohama 226-8503, Japan.

[c] Department of Chemical System Engineering, University of Tokyo, 7-3-1 Hongo, Bunkyo-ku, Tokyo 113-8656, Japan.

*Email: yamag@res.titech.ac.jp

Electronic Supplementary Information (ESI) available: More detailed information on the calculations and the experimental analysis is provided in the ESI.

1. L. R. Merte, G. W. Peng, R. Bechstein, F. Rieboldt, C. A. Farberow, L. C. Grabow, W. Kudernatsch, S. Wendt, E. Laegsgaard, M. Mavrikakis and F. Besenbacher, *Science*, 2012, **336**, 889-893.

2. S. Wendt, J. Matthiesen, R. Schaub, E. K. Vestergaard, E. Lægsgaard, F. Besenbacher and B. Hammer, *Phys. Rev. Lett.*, 2006, **96**, 066107.
3. B. Musset, S. M. E. Smith, S. Rajan, D. Morgan, V. V. Cherny and T. E. DeCoursey, *Nature*, 2011, **480**, 273-278.
4. T. E. Decoursey, *Physiol. Rev.*, 2003, **83**, 475-579.
5. D. Voet, J. G. Voet, C. W. Pratt, in *Fundamentals of Biochemistry: Life at the Molecular Level*, Wiley, Hoboken, 4th edn., 2012, ch. 18, pp.604-612.
6. D. Marx, *ChemPhysChem*, 2006, **7**, 1848-1870.
7. R. Pomès and B. Roux, *Biophys. J.*, 2002, **82**, 2304-2316.
8. N. Agmon and M. Gutman, *Nat. Chem.*, 2011, **3**, 840-842.
9. Y. Georgievskii, E. S. Medvedev and A. A. Stuchebrukhov, *Biophys. J.*, 2002, **82**, 2833-2846.
10. Y. Marantz, E. Nachliel, A. Aagaard, P. Brzezinski and M. Gutman, *Proc. Natl. Acad. Sci. U. S. A.*, 1998, **95**, 8590-8595.
11. S. Checover, E. Nachliel, N. A. Dencher and M. Gutman, *Biochem.*, 1997, **36**, 13919-13928.
12. K. D. Kreuer, *Chem. Mat.*, 1996, **8**, 610-641.
13. T. Ogawa, H. Ushiyama, J. M. Lee, T. Yamaguchi and K. Yamashita, *J. Phys. Chem. C*, 2011, **115**, 5599-5606.
14. L. Vilciauskas, M. E. Tuckerman, G. Bester, S. J. Paddison and K. D. Kreuer, *Nat. Chem.*, 2012, **4**, 461-466.
15. M. Eikerling and A. A. Kornyshev, *J. Electroanal. Chem.*, 2002, **528**, 196-197.
16. S. J. Paddison, *Ann. Rev. Mater. Res.*, 2003, **33**, 289-319.
17. M. Eikerling, A. A. Kornyshev, A. M. Kuznetsov, J. Ulstrup and S. Walbran, *J. Phys. Chem. B*, 2001, **105**, 3646-3662.
18. K. D. Kreuer, S. J. Paddison, E. Spohr and M. Schuster, *Chem. Rev.*, 2004, **104**, 4637-4678.
19. W. Kulig and N. Agmon, *Nat. Chem.*, 2013, **5**, 29-35.
20. D. Marx, A. Chandra and M. E. Tuckerman, *Chem. Rev.*, 2010, **110**, 2174-2216.
21. N. Agmon, *J. Phys. Chem. A*, 2005, **109**, 13-35.
22. D. Marx, M. E. Tuckerman, J. Hutter and M. Parrinello, *Nature*, 1999, **397**, 601-604.
23. N. Agmon, *Chem. Phys. Lett.*, 1995, **244**, 456-462.
24. G. A. Voth, *Accounts Chem. Res.*, 2006, **39**, 143-150.
25. T. Ogawa, H. Ohashi, T. Tamaki and T. Yamaguchi, *Phys. Chem. Chem. Phys.*, 2013, **15**, 13814-13817.
26. T. C. Berkelbach, H. S. Lee and M. E. Tuckerman, *Phys. Rev. Lett.*, 2009, **103**, 238302
27. N. Agmon, *Biophys. J.*, 2005, **88**, 2452-2461.
28. T. Ogawa, T. Tamaki, H. Ohashi, H. Ushiyama, K. Yamashita, T. Yamaguchi, presented in part at the 62nd Annual International Society of Electrochemistry Meeting, Niigata, Japan, September 2011.
29. T. Ogawa, T. Tamaki, H. Ohashi, H. Ushiyama, K. Yamashita, T. Yamaguchi, Proceedings of the 10th International Symposium on Electrokinetic Phenomena, Tsukuba, Japan, 2012.
30. G. Alberti, M. Casciola, M. Pica, T. Tarpanelli and M. Sganappa, *Fuel Cells*, 2005, **5**, 366-374.
31. V. Di Noto, M. Piga, G. A. Giffin, K. Vezzu and T. A. Zawodzinski, *J. Am. Chem. Soc.*, 2012, **134**, 19099-19107.
32. J. M. Lee, G. M. Anilkumar, and T. Yamaguchi, presented in part at International Congress on Membnranes and Membrane Process 2005, Seoul, Korea, August, 2005.
33. M. Casciola, G. Alberti, A. Ciarletta, A. Cruccolini, P. Piaggio and M. Pica, *Solid State Ionics*, 2005, **176**, 2985-2989.
34. G. Alberti, M. Casciola, D. Capitani, A. Donnadio, R. Narducci, M. Pica and M. Sganappa, *Electrochim. Acta*, 2007, **52**, 8125-8132.
35. G. Alberti and M. Casciola, *Ann. Rev. Mater. Res.*, 2003, **33**, 129-154.
36. M. Aparicio and L. C. Klein, *J. Electrochem. Soc.*, 2005, **152**, A493-A496.
37. T. M. Thampan, N. H. Jalani, P. Choi and R. Datta, *J. Electrochem. Soc.*, 2005, **152**, A316-A325.
38. J. M. Lee, Y. Kikuchi, H. Ohashi, T. Tamaki and T. Yamaguchi, *J. Mater. Chem.*, 2010, **20**, 6239-6244.
39. J. M. Soler, E. Artacho, J. D. Gale, A. Garcia, J. Junquera, P. Ordejon and D. Sanchez-Portal, *J. Phys.-Condes. Matter*, 2002, **14**, 2745-2779.
40. B. Hammer, L. B. Hansen and J. K. Norskov, *Phys. Rev. B*, 1999, **59**, 7413-7421.
41. J. Junquera, O. Paz, D. Sanchez-Portal and E. Artacho, *Phys. Rev. B*, 2001, **64**, 235111.
42. N. Gonzalez-Garcia, J. Z. Pu, A. Gonzalez-Lafont, J. M. Lluch and D. G. Truhlar, *J. Chem. Theory Comput.*, 2006, **2**, 895-904.
43. G. Henkelman, B. P. Uberuaga and H. Jonsson, *J. Chem. Phys.*, 2000, **113**, 9901-9904.
44. T. Ohto, I. Rungger, K. Yamashita, H. Nakamura and S. Sanvito, *Phys. Rev. B*, 2013, **87**, 205439.
45. S. Changkhamchom and A. Sirivat, *Polymer Bulletin*, 2010, **65**, 265-281.
46. P. Atkins, J. Paula, in *Atkins' Physical Chemistry*, Oxford University Press, New York, 9th edn., 2009, ch. 20, pp. 758-759, 763, 768-769.
47. W. B. Lewis, M. Alei and L. O. Morgan, *J. Chem. Phys.*, 1966, **44**, 2409-2417.
48. S. Nose, *Mol. Phys.*, 1984, **52**, 255-268.
49. Hara, N.; Ohashi, H.; Ito, T. and Yamaguchi, T. *J. Phys. Chem. B* 2009, **113**, 4656-4663.